https://doi.org/10.1016/j.ijmecsci.2017.07.046

Study of deformation and ductile fracture behaviors in micro-scale deformation using a combined surface layer and grain boundary strengthening model

W.T. Li[a], M.W. Fu[a, b, *], S.Q. Shi[a]

[a] Department of Mechanical Engineering, The Hong Kong Polytechnic University, Hung Hom, Kowloon, Hong Kong

[b] PolyU Shenzhen Research Institute, No.18 Yuexing Road, Nanshan District, Shenzhen, P.R. China

* Email: mmmwfu@polyu.edu.hk, Tel: +852-27665527

Abstract

A constitutive model considering the composition of surface grain, grain boundary and grain interior and their contributions to the flow stress or strength of materials in micro-scale plastic deformation is developed and termed as a combined surface layer and grain boundary strengthening model in this research. To determine the composition of the three interior microstructural parts of materials, optical microscope and digital image processing technologies are employed. A series of micro-tensile experiments using the specimens with three different geometrical shapes and microstructural grain sizes are conducted for study of deformation and ductile fracture behaviors of material. The model is implemented in finite element analysis and validated via physical experiments. The relationship among fracture strain, grain size and stress triaxiality of the deforming material is thus established. It is found both fracture strain and stress triaxiality increase with the decrease of grain size, while the high stress triaxiality leads to small fracture strain for the given grain size. Through observation of the fractographs, it is revealed that the domination of shear fracture in the 'cup-cone' fracture increases with grain size. The research thus helps understand the ductile fracture in micro-scale deformation and facilitates deformation based working process determination and application.

Keywords: Constitutive model, Grain size effect, Ductile fracture, Stress triaxiality, Micro-scale deformation

1. Introduction

Nowadays, micro-scale parts have been widely used in many industrial applications such as consumer electronic, watch and jewelry, biomedical devices and system, and micro-electro-mechanical system (MEMS), etc. and they are increasingly demanded due to newly emerging requirements from different aspects such as material and energy saving, weight and volume decreasing, environmental impact reducing and product portability increasing [1, 2]. To produce micro-scaled metallic parts on a large scale, deformation based micro-manufacturing is one of the efficient approaches. In this process, ductile fracture (DF) is a critical phenomenon to be considered as it affects the geometry and shape of forming of micropart and its quality and property tailoring. DF is thus critical in design of fracture resistant process, determination of the formability of material and quality assurance of defect-free parts [3-5]. DF in micro-scale deformation process, on the other hand, differs from that in macro-scale mainly due to the size effects arising from different sources including variation of material geometry size and microstructural grain size on the deformation behavior, material flow, surface quality, shape accuracy, dimension accuracy and defect formation [6, 7]. In-depth understanding of the fracture mechanism, mode and behavior of DF would facilitate the development of deformation based micro-manufacturing process.

DF and the deformation exist simultaneously in the deformation based working process of materials. Both need to be extensively considered concurrently for exploring DF in micro-scale. Some researchers have made their efforts to address this issue in the past few decades. To name a few, a mixed constitutive model built on the surface layer model by combining the

theories of single-crystal and polycrystal was established by Lai et al. [8]. In their model, the properties of single-crystal and polycrystal almost represent those of surface and inner grains, respectively. A new composite model employed to show the impact of dimension, shape and grain size of specimen on plastic deformation was built by Shen and Yu [9]. They concluded that the decrease amount of the strength of material is slowly increased with the decreased billet dimension and the increased grain size. The section shape of billet plays a critical role on it as well. The decrease amount of the strength of billet with circular cross-section shows smaller than that of billet with rectangular cross-section in the same section area. According to the composite model and the surface layer model, Liu et al. [10] developed a new model to figure out the mechanical behavior of polycrystal. Grain boundary and grain interior are two portions in the microstructure of material, with an assumption that the mechanical behaviors of surface grain and grain interior are closely equal. The simulation by employing their model is consistent with the physical experiment. For investigation of size effect on the micro-scale amorphous polymers, Deng et al. [11] came up with an "elastic-viscoplastic" constitutive model with a consideration of rotational strain gradient. It was verified and validated by four-point micro-bending experiment of Poly (methyl methacrylate). In addition, Ran et al. [12] introduced the size factor into Freudenthal fracture criterion by considering surface layer model. They found that the ductile fracture happens in macroforming scenario, while it occurs with difficulty in microforming when the deformation conditions are same. In other words, the fracture strain is larger in the same deformation condition with the smaller sample size in micro-scale deformation. Gruben et al. [13] evaluated the modified Mohr-Coulomb and the extended Cockcroft-Latham and Rice-Tracey fracture criteria, which obviously explain the Lode dependence and the stress triaxiality on damage evolution. Through comparing the predicted equivalent strain at fracture initiation based on the modified and extended fracture criteria with the experimental results, they revealed that the extended

Cockcroft-Latham criterion has a better prediction of the fracture strain compared to that of the extended Rice-Tracey and the modified Mohr-Coulomb criteria with a large deviation. The research, however, is more on macro-scale deformation and its validity in micro-scale deformation has not been explored. From both macro- and micro-scale deformations, the analysis and prediction of DF via consideration of surface grain, grain interior and grain boundary and their deformation behaviors in fracture formation have not yet been found based on the available literatures and this is the endeavor of this research, especially focused on micro-scale plastic deformation of materials.

From fracture formation aspect, some researchers have paid more attentions to fractographic features in ductile fracture. Li et al. [4] compared the fractographs of upsetting samples with those of tensile test samples to obtain the mesoscopic ductile fracture behavior and formation mechanism. Their observation revealed that shear-dimple ductile fracture mode exists in upsetting and tensile test samples and the stress triaxiality affects the ductile fracture mode. Shear ductile fracture occurs when the stress triaxiality is below zero. Both shear ductile fracture and void-growth ductile fracture exist together and compete with each other when the stress triaxiality is from zero to 1/3. Void-growth ductile fracture dominates when the stress triaxiality is more than 1/3. Toulfatzis et al. [14] analyzed the dimple size and distribution on fractographs of all the tested brass alloys. They found that the finest and shallowest shear dimples on the fracture surface of the CW614N leaded brass are observed, whereas the largest and deepest dimples are illustrated in the brass alloys CW511L and C27450 with absorbing the highest impact energy. Das et al. [15] employed digital image processing to determine the dimple network according to the fractographs of all the specimens. Their study indicated that there is a strong relationship among fractographic features, dimple size and density and mechanical properties. Similarly, the fractographic

features on the fracture cross-section of the micro-scale specimen will be observed to analyze the fracture mode and mechanism.

In this research, a combined surface layer and grain boundary strengthening model by considering the contributions of surface grain, grain boundary and grain interior to mechanical behavior of material is developed in micro-scale plastic deformation. The physical experiments and finite element (FE) simulations of micro-tensile specimens with three different geometrical shapes and microstructural grain sizes are employed to validate the efficiency of the model. The relationship of grain size, fracture strain and stress triaxiality is thus established based on physical experiment and FE simulation by employing the newly combined constitutive model. Finally, the fractographs of the micro-tensile specimens with different grain sizes and geometrical shapes are analyzed, especially for the size and distribution of dimple in the fracture cross-section. This paper thus facilitates to advance the knowledge of deformation and ductile fracture in micro-scale deformation based working process, especially for the interaction of stress triaxiality, fracture strain and grain size and their influences on fracture formation.

2. Developed constitutive model and research methodology

2.1 Surface layer model

Surface and inner grains co-exist in the deformation body based on the surface layer model. Surface grains are easier to deform mainly due to few constraints compared with inner grains which have more constraints. The strength of material can be formulated below:

$$\begin{cases} \sigma = f_{surf}\sigma_{surf} + f_{inner}\sigma_{inner} \\ 1 = f_{surf} + f_{inner} \end{cases} \tag{1}$$

In Eq. (1) σ is the flow stress of material. σ_{surf} and f_{surf} are the flow stress and the fraction of surface grains, while σ_{inner} and f_{inner} are the flow stress and the fraction of inner grains, respectively.

Based on the surface layer model discussed above, a mixed constitutive model in which the flow stresses of surface and inner grains are closely equal to those of single crystal and polycrystal, respectively, was proposed by Lai et al. [8]. The single crystal model can be expressed as follows in accordance with single crystal theory and the Schmid law, also shown by Lai et al. [8] and Kim et al. [16],:

$$\sigma_{sig}(\varepsilon) = \frac{\tau_R(\varepsilon)}{\cos\varphi\cos\lambda} = m\tau_R(\varepsilon) \ (m\geq 2) \tag{2}$$

where $\sigma_{sig}(\varepsilon)$ and $\tau_R(\varepsilon)$ are the flow stress of single crystal and the critical resolved shear stress, respectively. φ is the angle between the normal stress and the normal direction of the slip plane and λ is the angle between the slip direction and the normal stress. In addition, m is the orientation factor.

For the polycrystal model, the Hall-Petch relationship extended by Armstrong [17] is widely employed to represent the flow stress [8, 12, 16, 18] in the following:

$$\sigma_{poly}(\varepsilon) = \sigma_0(\varepsilon) + \frac{k(\varepsilon)}{\sqrt{d}} = M\tau_R(\varepsilon) + \frac{k(\varepsilon)}{\sqrt{d}} \tag{3}$$

where $\sigma_{poly}(\varepsilon)$ is the polycrystal flow stress. $\sigma_0(\varepsilon)$ and $k(\varepsilon)$ are constants for a given strain (ε). d is the grain size and M is the orientation factor with the value of 3.06 and 2.23 for face centered cubic crystals in the Taylor and Sachs models, respectively [19].

Therefore, the mixed material model by combining Eqs. (2) and (3) proposed by Lai et al. [8] consists of two parts as follows:

$$\begin{cases} \sigma_{surf}(\varepsilon) = m\tau_R(\varepsilon) \\ \sigma_{inner}(\varepsilon) = M\tau_R(\varepsilon) + \frac{k(\varepsilon)}{\sqrt{d}} \end{cases} \tag{4}$$

2.2 Grain boundary strengthening model

Actually, many researchers attracted by the characteristics of grain boundary have explored the material strengthening. According to Meyersm and Ashworth [20], polycrystalline aggregate is composed of grain interior and grain boundary. Hirth [21] mentioned that higher strain hardening can be generated by grain boundary compared with grain interior. The main reason is that grain boundary forbids the propagation of slip, further generating the pile-up of dislocation and strain hardening, leading to the high strength of materials in this location, also reported by Chan et al. [22]. The strength of polycrystal can be calculated as follows in the form of a composite model based on Meyersm and Ashworth [20] and Kocks [23]:

$$\begin{cases} \sigma_{poly} = f_{gb}\sigma_{gb} + f_{gi}\sigma_{gi} \\ 1 = f_{gb} + f_{gi} \end{cases} \tag{5}$$

where σ_{poly} is the flow stress of polycrystalline aggregate. σ_{gb} and f_{gb} are the flow stress and the area fraction of the grain boundary, while σ_{gi} and f_{gi} are the flow stress and the area fraction of the grain interior, respectively. In grain boundary strengthening model, the material is supposed to contain grain interior and grain boundary, while the grains are classified into surface and inner grains in surface layer model. The surface grains are defined as those located at the outer layer of the material, while inner grains are those in the inner part.

It is critical to describe the flow stresses of grain boundary and grain interior in accordance with the above model. Swygenhoven et al. [24] and Gleiter [25] reported that the amorphous structure of atom almost occurs at grain boundary based on atomic simulation. For the amorphous material, Donovan [26] proved that Drucker's constitutive equation [27] is able

to simulate the plastic deformation behavior. Jiang and Weng [28, 29] and Zhou et al. [30] thus employed the Drucker's constitutive equation to present the flow stress of grain boundary as follows:

$$\sigma_{gb}(\varepsilon_{gb}^{p}) = \sigma_{y}^{gb} + np + h_{gb}(\varepsilon_{gb}^{p})^{n_{gb}} \tag{6}$$

where $\sigma_{gb}(\varepsilon_{gb}^{p})$, σ_{y}^{gb} and ε_{gb}^{p} are the flow stress, yield stress and plastic strain of grain boundary. n, h_{gb} and n_{gb} are material constants of grain boundary. Furthermore, $p = -\frac{1}{3}(\sigma_1 + \sigma_2 + \sigma_3)$ is the hydrostatic pressure and σ_1, σ_2 and σ_3 are the first, second and third principal stresses, respectively.

According to Weng [31], grain size affects the plastic deformation in constituent grain because of the possible pile-up of dislocation and the dislocation substructures in grain boundary. The mechanical property of grain interior in accordance with the mixed isotropic hardening law can be formulated as [28-30]:

$$\begin{cases} \sigma_{gi}(\varepsilon_{gi}^{p}) = \sigma_{y}^{gi} + h_{gi}(\varepsilon_{gi}^{p})^{n_{gi}} \\ \sigma_{y}^{gi}(d) = \sigma_{y}^{\infty(gi)} + kd^{-1/2} \\ h_{gi}(d) = h_{gi}^{\infty} + ad^{-1/2} \end{cases} \tag{7}$$

where $\sigma_{gi}(\varepsilon_{gi}^{p})$, σ_{y}^{gi}, h_{gi}, ε_{gi}^{p} and n_{gi} are the flow stress, initial yield stress, strength coefficient, plastic strain and work hardening exponent of grain interior. In addition, $\sigma_{y}^{gi}(d)$ and $h_{gi}(d)$ are expressed with the grain size d, which are similar in form to Hall-Petch relationship. $\sigma_{y}^{\infty(gi)}$, k, h_{gi}^{∞} and a are material constants in terms of the single crystal or the grain with infinite size.

2.3 The developed constitutive model

In the mixed constitutive model proposed by Lai et al. [8], the specimen is assumed to consist of surface and inner grains, whose mechanical properties are similar to those of single crystal and polycrystalline aggregate, respectively. Inner grain which has the same plastic behavior with polycrystalline aggregate thus can be divided into grain interior and grain boundary on the basis of grain boundary strengthening model proposed by Meyersm and Ashworth [20] and Kocks [23]. Therefore, the specimen material has three portions in this research, viz., surface grain, grain interior and grain boundary. The following equations can thus represent the flow stress of material:

$$\begin{cases} \sigma = f_{surf}\sigma_{surf} + f_{gb}\sigma_{gb} + f_{gi}\sigma_{gi} \\ 1 = f_{surf} + f_{gb} + f_{gi} \end{cases} \tag{8}$$

Additionally, there is an assumption that the plastic strains of grain boundary and grain interior are equal in accordance with the iso-strain model [22]. Combining Eqs. (2), (6) and (7) into Eq. (8), the formula for the developed constitutive model in this research is put forward in the following:

$$\begin{cases} \sigma(\varepsilon) = f_{surf} m \tau_R(\varepsilon) + f_{gb}\left(\sigma_y^{gb} + np + h_{gb}\varepsilon^{n_{gb}}\right) + f_{gi}(\sigma_y^{\infty(gi)} + kd^{-1/2} + (h_{gi}^{\infty} + ad^{-1/2})\varepsilon^{n_{gi}}) \\ 1 = f_{surf} + f_{gb} + f_{gi} \end{cases} \tag{9}$$

where $\sigma(\varepsilon)$ represents the flow stress of the specimen material.

2.4 Research methodology

Fig. 1 shows the research methodology by which a combined surface layer and grain boundary strengthening model employed to simulate and analyze the deformation behavior and ductile fracture in micro-scale deformation is developed. To validate the proposed model and its application in different deformation scenarios, three different geometrical shapes of pure copper specimens with the effective diameter of 1 mm are annealed at 400, 750 and

1000 ºC for 3, 1 and 1 hours, respectively, to produce different microstructural grain sizes. The dog-bone samples with different grain sizes are employed to carry out micro-tensile tests to determine the true stress-strain curves of the materials. The metallographs with different microstructures and grain sizes, which are observed by optical microscope, are used to extract information, viz. area fractions of surface grain, grain interior and grain boundary based on the digital image processing technology. The combined surface layer and grain boundary strengthening model is thus built, in which the mechanical property of surface grain is established by the surface layer model and the flow stresses of grain interior and grain boundary are formulated by the grain boundary strengthening model. On the basis of the combined constitutive model, FE simulation is conducted to simulate the whole micro-tensile test by importing the material property, meshing the tensile deformation sample, setting up boundary condition, etc. Furthermore, the load-displacement curves determined by physical experiments and FE simulations are compared to validate the newly combined constitutive model. In accordance with the physical experiments and FE simulations using the proposed constitutive model, the interactive relationship of grain size, stress triaxiality and fracture strain can be established in this research. Finally, fractographs are observed to explore the fracture mechanism and mode in the deformation process. All of these intend to more accurately predict the ductile fracture and advance the knowledge of the interaction among grain size, fracture strain and stress triaxiality in micro-scale deformation and their effects on fracture formation in the deformation.

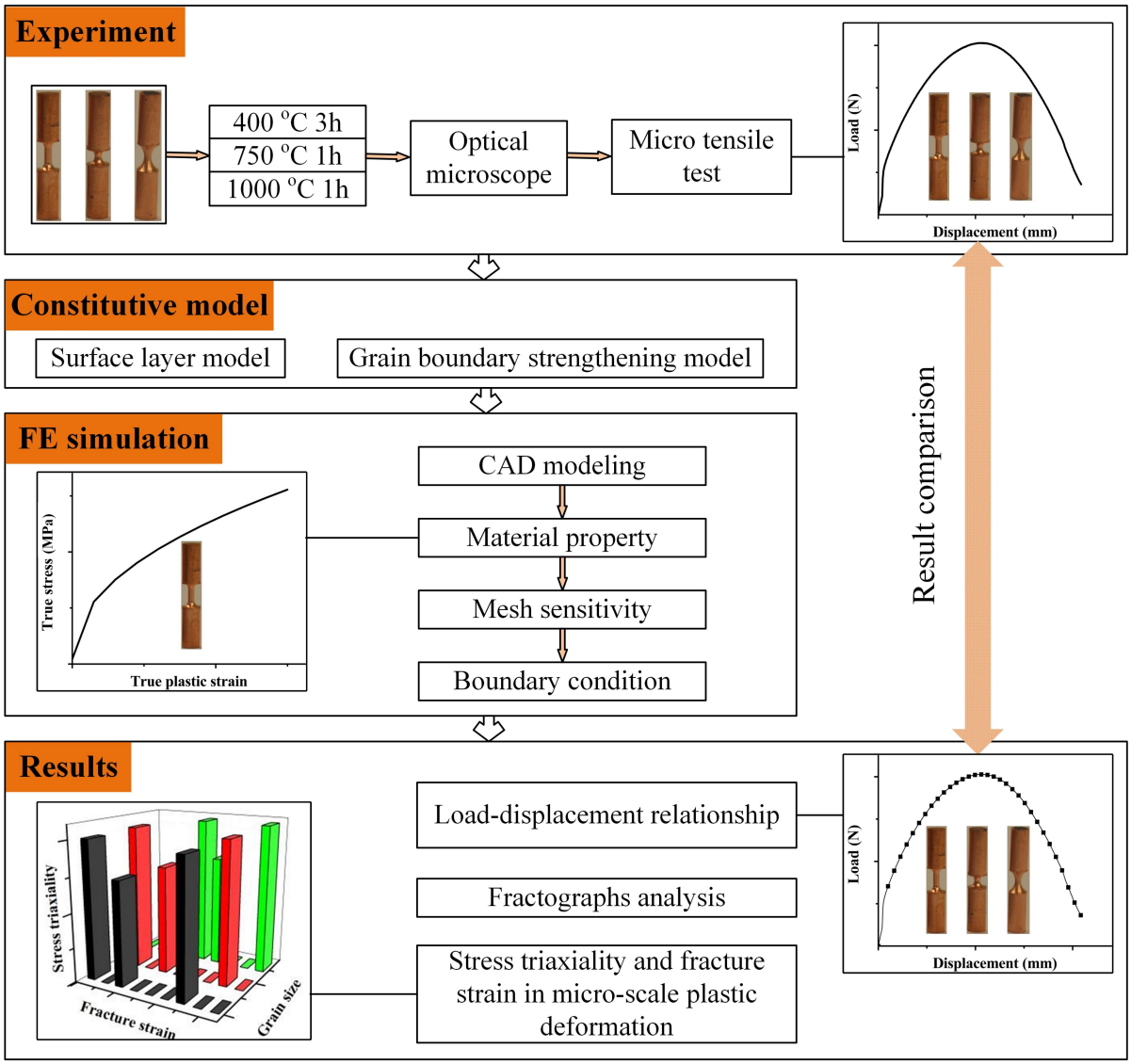

Fig. 1 Research flow of the newly combined constitutive model.

3. Experimental procedure

3.1. Grip design and specimen preparation

It can be seen from the Fig. 2 that a set of grips and the tiny dog-bone specimen have been smartly designed and manufactured to facilitate the micro-tensile tests. In addition, the selected research material is pure copper because of its good ductility and extensive use. The pure copper specimens are annealed in the argon atmosphere for protection against oxidation at 400, 750 and 1000 °C for 3, 1 and 1 hours, respectively. The microstructures of annealed

specimens can thus be observed by optical microscope after they are polished and etched in the etchant of 5 g $FeCl_3$, 85 mL H_2O and 15 mL HCl for 18~25 seconds, as displayed in Fig. 3.

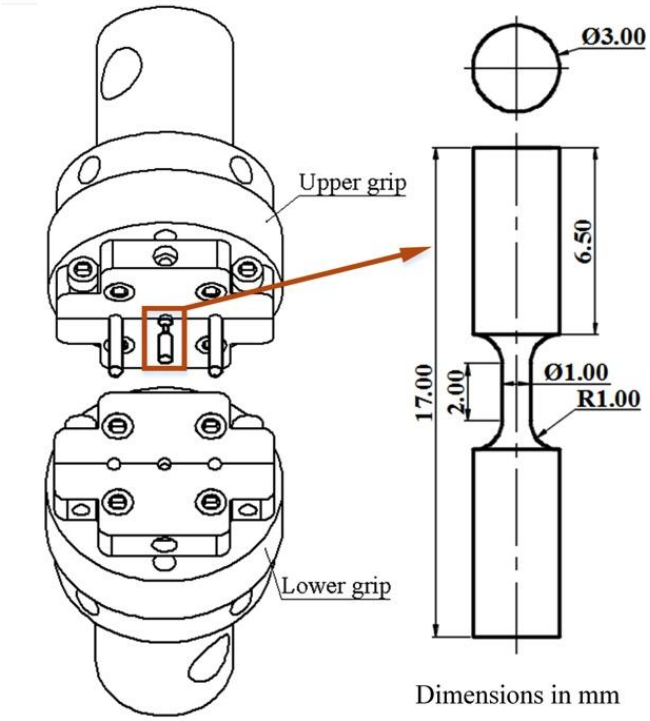

Fig. 2 A set of grips and the tiny dog-bone specimen.

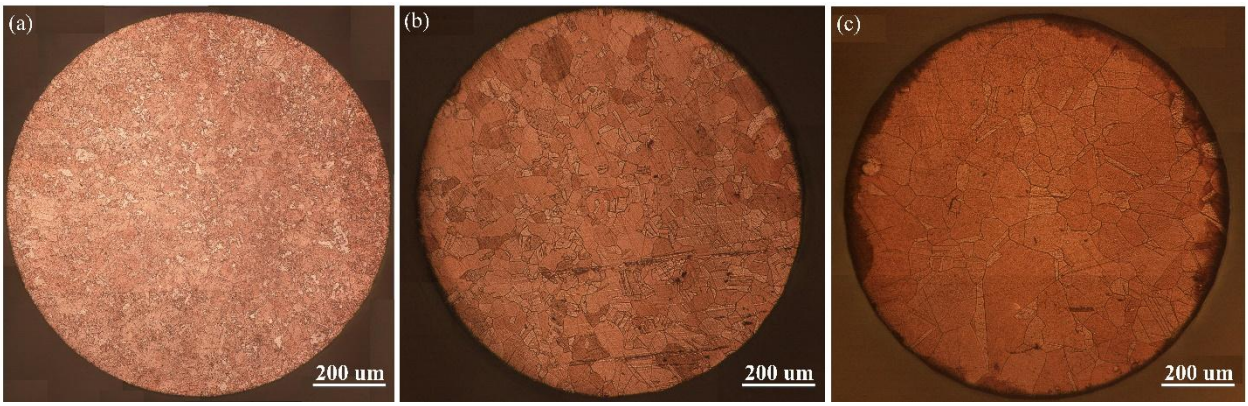

Fig. 3 Microstructures of the specimens after heat treatment at (a) 400 °C; (b) 750 °C and (c) 1000 °C for 3, 1 and 1 hours, respectively.

3.2. Processing and analysis of metallographs

The metallography with different microstructural grain sizes is obtained. The software ArcMap is used to extract information to calculate the area ratios of surface grain, grain interior and grain boundary using digital image processing technology, as shown in Fig. 4. Generally, each metallograph is a raster layer which can be processed to extract vector features, such as points, polylines, and polygons, which summarize the interesting information, such as total number of grains, area or perimeter of each grain, etc. by the digital image processing method. Firstly, an image containing brighter grains with higher gray values and darker grain boundary with lower gray values is chosen. A threshold is thus determined to separate the grain and grain boundary. Unfortunately, it is not able to precisely detect the outer circular boundary of the specimen for over oxidation. To solve this problem, an inner fence and surface grains are digitalized manually and recorded as a single polygon and a set of spatial contiguous polygons, respectively, so that information of the digitalized surface grains can be summarized and pixels out of the fence are discarded. Further, the digitalized surface grains are converted to overlap with the maintained inner part as a combined raster layer of grain boundary, and pixel resolution of this raster layer equals the averaged width of the boundary. The raster layer can be converted as an editable vector layer to cut and remove the noises. Finally, the raster layer grouped by grain interior, surface grain and grain boundary is obtained to calculate the area fractions by accumulating the area of pixels, shown in the end of Fig. 4. Fig. 5 shows the schematic diagram of calculating the fractions of grain boundary and surface grain for the sample annealed at 1000 ^{o}C with the holding time of 1 hour. Table 1 presents the area ratios of grain interior, surface grain and grain boundary of the samples annealed at 400, 750 and 1000 ^{o}C for 3, 1 and 1 hours, respectively.

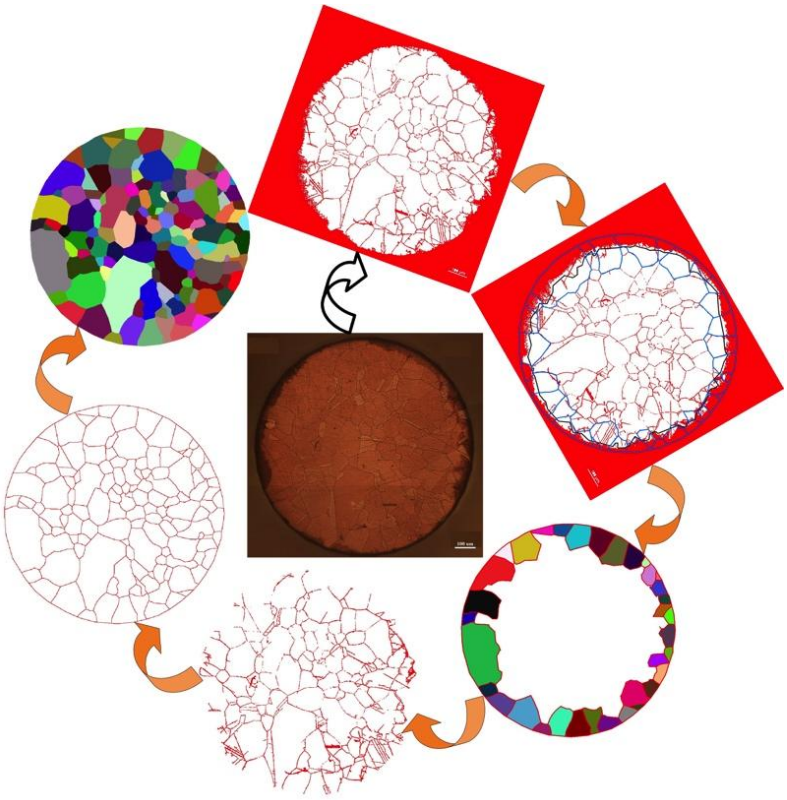

Fig. 4 Digital image processing to extract the raster layer grouped by grain interior, surface grain and grain boundary.

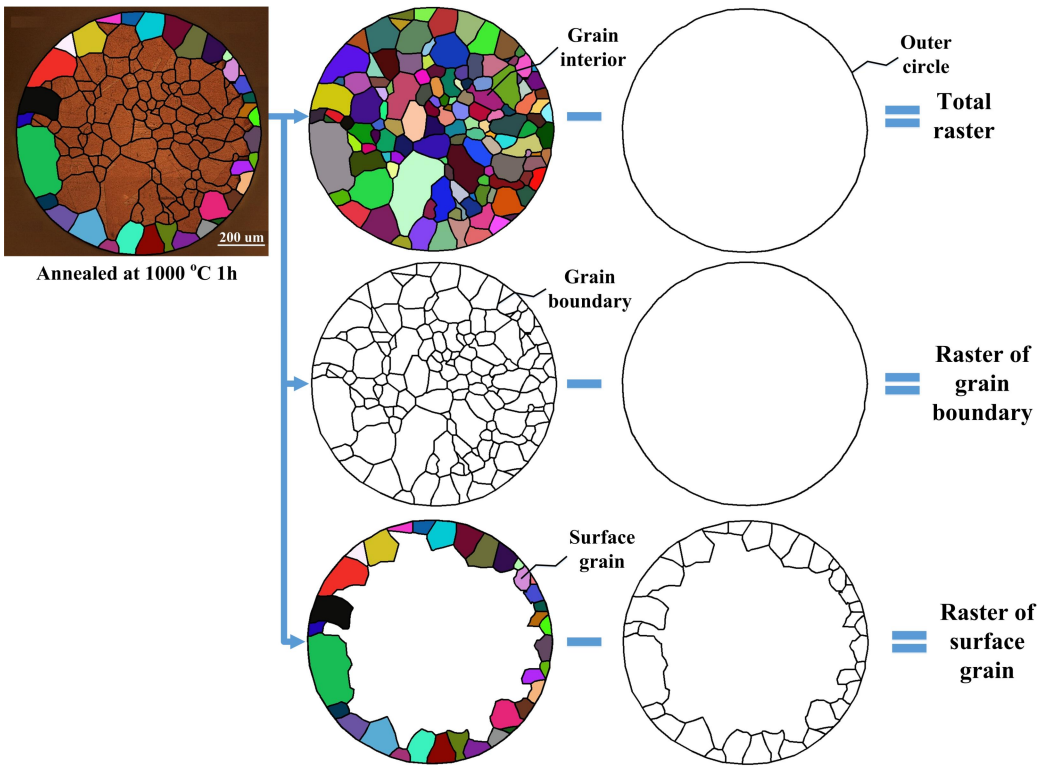

Fig. 5 Schematic diagram of the determination of area ratios of grain boundary and surface grain for the sample annealed at 1000 °C for 1 hour.

Table 1 Fractions of grain interior, surface grain and grain boundary.

Material condition	Fraction of surface grain	Fraction of grain boundary	Fraction of grain interior	Mean grain size (um)
400 °C for 3 hours	2.80%	23.06%	74.14%	8.23
750 °C for 1 hour	19.93%	8.85%	71.22%	41.78
1000 °C for 1 hour	32.78%	4.17%	63.05%	79.36

3.3 Experimental setup

An experimental platform on the top of a MTS system is established and the system automatically takes photos with an extremely fine resolution with a fixed time interval to record the whole micro-scale deformation process. The true stress and strain relationship is determined based on the recorded loading of the MTS system and the displacement from the photos taken during the micro-tensile test. Fig. 6 shows the whole micro-tensile process of the tiny dog-bone specimen and Fig. 7 displays the true stress-strain curves of the dog-bone samples with three different microstructural grain sizes. The true stress-strain curves of the three different geometrical shapes of pure copper specimens with the same grain size are considered to be equal in this research. Furthermore, the decrease of flow stress in Fig. 7 can be explained by the surface layer and grain boundary strengthening models. In the grain boundary strengthening model, grain boundary forbids the propagation of slip, further generating the pile-up of dislocation and strain hardening, leading to the higher strength of material in this location. The specimen with a larger grain size and less number of grains in the cross section has a relatively lower density of grain boundary, which results in a lower restriction to deformation and the lower flow stress. The characteristics of grain boundary thus have a close relationship with grain size effect on the deformation of material, also reported by Chan et al. [32]. According to the surface layer model, the surface grains have fewer constraints to deformation and thus have a lower stress compared with inner grains. For the dog-bone specimens with the same thickness, the area fraction of surface grains in cross section increases with grain size, which causes the decrease of flow stress. When the grain

size keeps constant, different geometrical sizes of specimens have different fractions of surface grains in the cross section and different tensile curves. Thus, the geometry size effect on the deformation of material can be explained by the surface layer model.

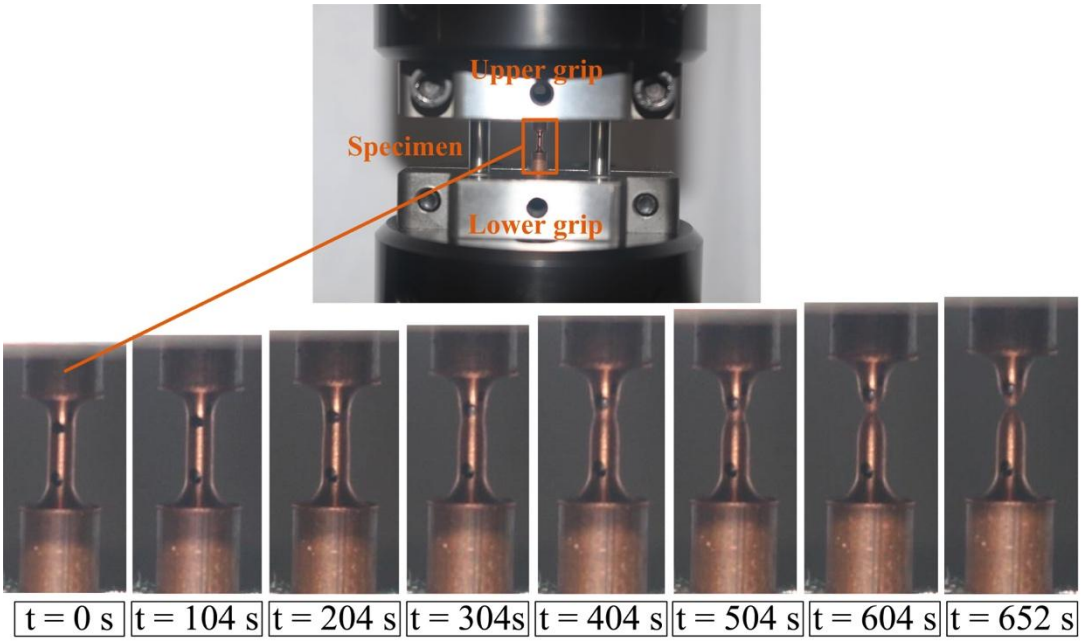

Fig. 6 The whole micro-tensile process of the tiny dog-bone specimen.

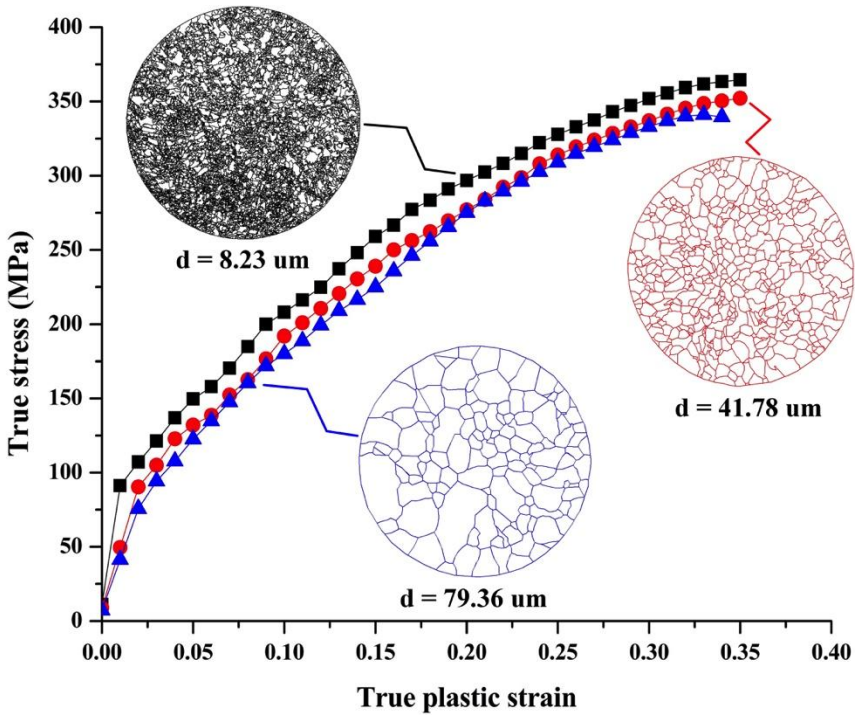

Fig. 7 True stress-strain relationships of the dog-bone samples with different microstructural grain sizes.

4. Simulation implementation and validation

4.1 Determination of the parameters in the newly combined constitutive model

To determine the parameters in the newly combined constitutive model, fitting curve method on the basis of the experimental flow stress-strain relationships introduced by Ran et al. [12, 18] is employed. When the strain keeps constant, grain size and flow stress can be formulated in the form of Hall-Petch relationship shown in Fig. 8 below. It can be seen that $M\tau_R$ is established based on the fitted linear function of flow stress and grain size for different strain values. Thus, the fitting curve of $M\tau_R$ and strain can be displayed in Fig. 9. It can be expressed as follows:

$$M\tau_R = 599.546\varepsilon^{0.535} \tag{10}$$

where M is equal to 3.06 in this article. Eq. (10) is combined with Eq. (4) to obtain the flow stress of surface grain according to the surface layer model:

$$\sigma_{surf}(\varepsilon) = m\tau_R(\varepsilon) = 391.86\varepsilon^{0.535} \tag{11}$$

where m is equal to the minimum value, viz. 2.

The area ratios of grain interior, surface grain and grain boundary and the mean grain size are determined based on the digital image processing technology mentioned above. For the determination of parameters in the formulas of mechanical properties of grain boundary and grain interior, n can be set to 0.4 as the material constant of the grain boundary for pure copper according to Zhou et al. [30]. When strain is equal to zero, $\sigma_y^{\infty(gi)}$, k and σ_y^{gb} are three unknowns in the newly combined constitutive model. The true stress-strain curves of the samples with three different microstructural grain sizes are thus needed to determine the three unknowns under the condition of zero strain. For the remaining five unknown coefficients, viz. h_{gi}^{∞}, h_{gb}, a, n_{gi} and n_{gb}, curve fitting method is employed. Firstly, the true stress-strain

curve of the sample annealed at 750 ºC is employed to obtain the five unknown coefficients by curve fitting mainly due to the appropriate fractions of grain interior and grain boundary. Secondly, the mechanical property of the specimen annealed at 1000 ºC is used to validate the newly combined constitutive model. Finally, the five unknown coefficients may need a slight adjustment to ensure a good matching between the physical experiment and the fitted curve for the sample annealed at 400 ºC. Therefore, the formulas of mechanical properties of grain boundary and grain interior are designated as:

$$\sigma_{gb}(\varepsilon) = 16.91 + 0.4p + 815.99\varepsilon^{0.47} \tag{12}$$

$$\sigma_{gi}(\varepsilon) = 10.57 - 1.21d^{-1/2} + (629.01 + 3.56d^{-1/2})\varepsilon^{0.47} \tag{13}$$

Fig. 10 exhibits the true stress-strain curves of grain interior, surface grain and grain boundary of the sample annealed at 750 ºC for 1 hour. Thus, combining Eqs. (11), (12) and (13) into Eq. (9), the developed constitutive model is thus expressed in the following:

$$\begin{cases} \sigma(\varepsilon) = f_{surf}391.86\varepsilon^{0.535} + f_{gb}(16.91 + 0.4p + 815.99\varepsilon^{0.47}) \\ \qquad + f_{gi}(10.57 - 1.21d^{-1/2} + (629.01 + 3.56d^{-1/2})\varepsilon^{0.47}) \\ 1 = f_{surf} + f_{gb} + f_{gi} \end{cases} \tag{14}$$

Fig. 11 presents the comparisons of experimental results and different constitutive models, viz. Ran's surface layer model [12] and the proposed constitutive model for the samples with different grain sizes. It can be seen from Fig. 11(a) that the fitted curve of Ran's model is closer to the experiment. It is mainly due to the different fractions of surface grains and the determination of the flow stress of inner part in the specimen. The fraction of surface grains is calculated based on the uniformly-distributed sphere model of grain in Ran's model, while it is determined by digital image processing technology for the combined constitutive model in this research. The flow stress of inner part, which represents the strength of polycrystal and is not related to feature size factor in Ran's model, is obtained from the nonlinear curve

fitting of the true stress-strain relationship of the specimen with the grain size of 8.23 um. However, grain boundary and grain interior are considered in the inner part of the specimen in the combined constitutive model, and the formulas of flow stresses of grain boundary and grain interior are derived from the true stress-strain curves of the samples with three different microstructural grain sizes. The accuracy of the combined constitutive model thus shows higher, especially for the specimen with a larger grain size.

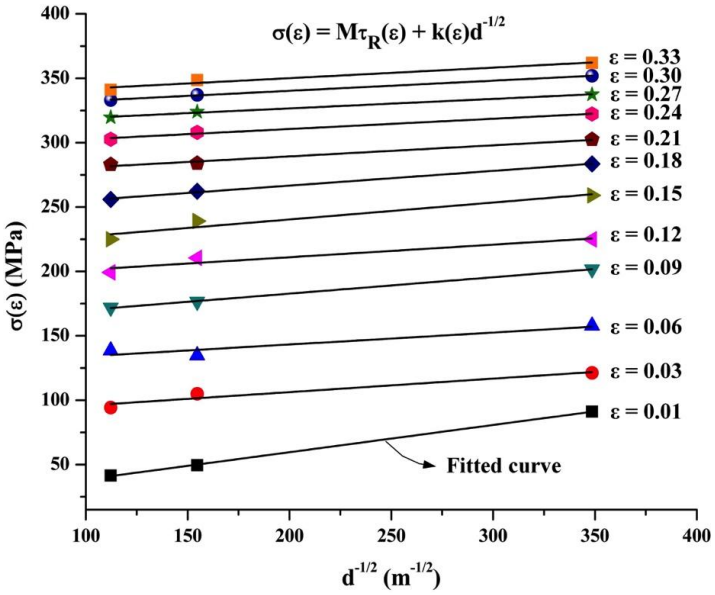

Fig. 8 Flow stress and grain size in the form of Hall-Petch equation.

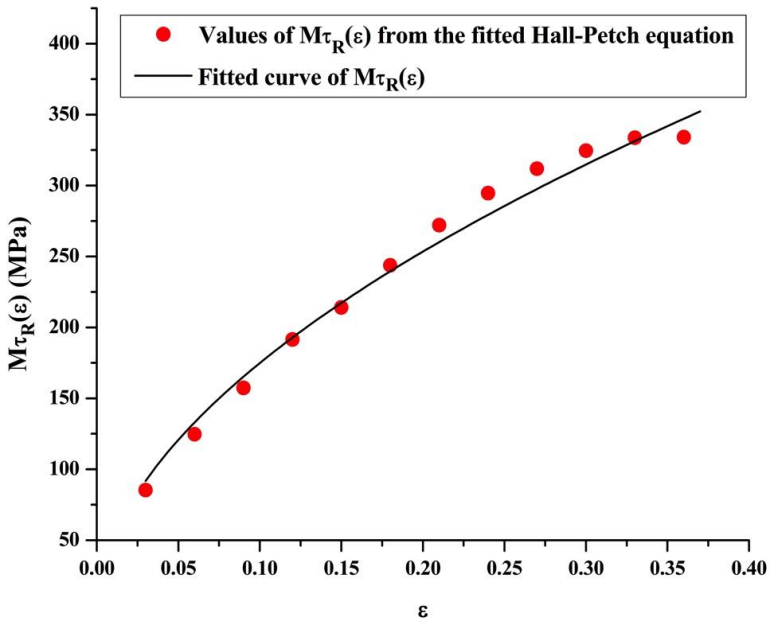

Fig. 9 Relationship of $M\tau_R(\varepsilon)$ and ε.

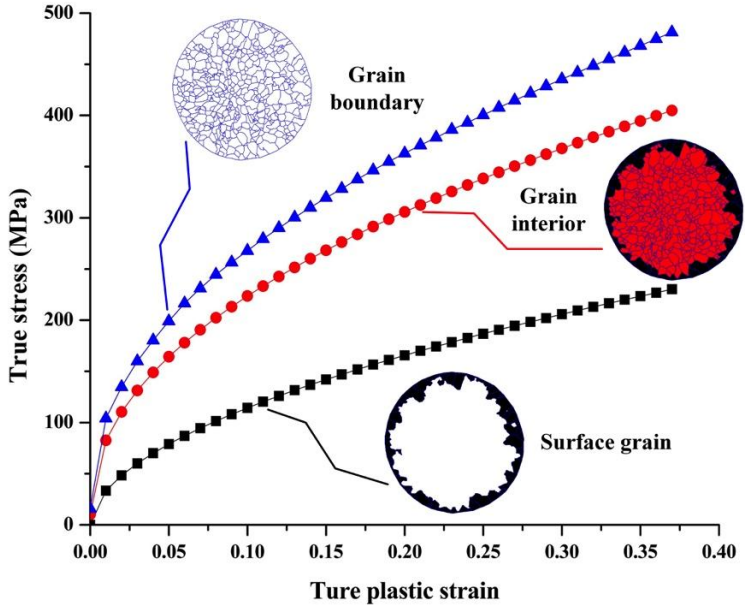

Fig. 10 True stress-strain curves of grain interior, surface grain and grain boundary of the sample annealed at 750 ºC.

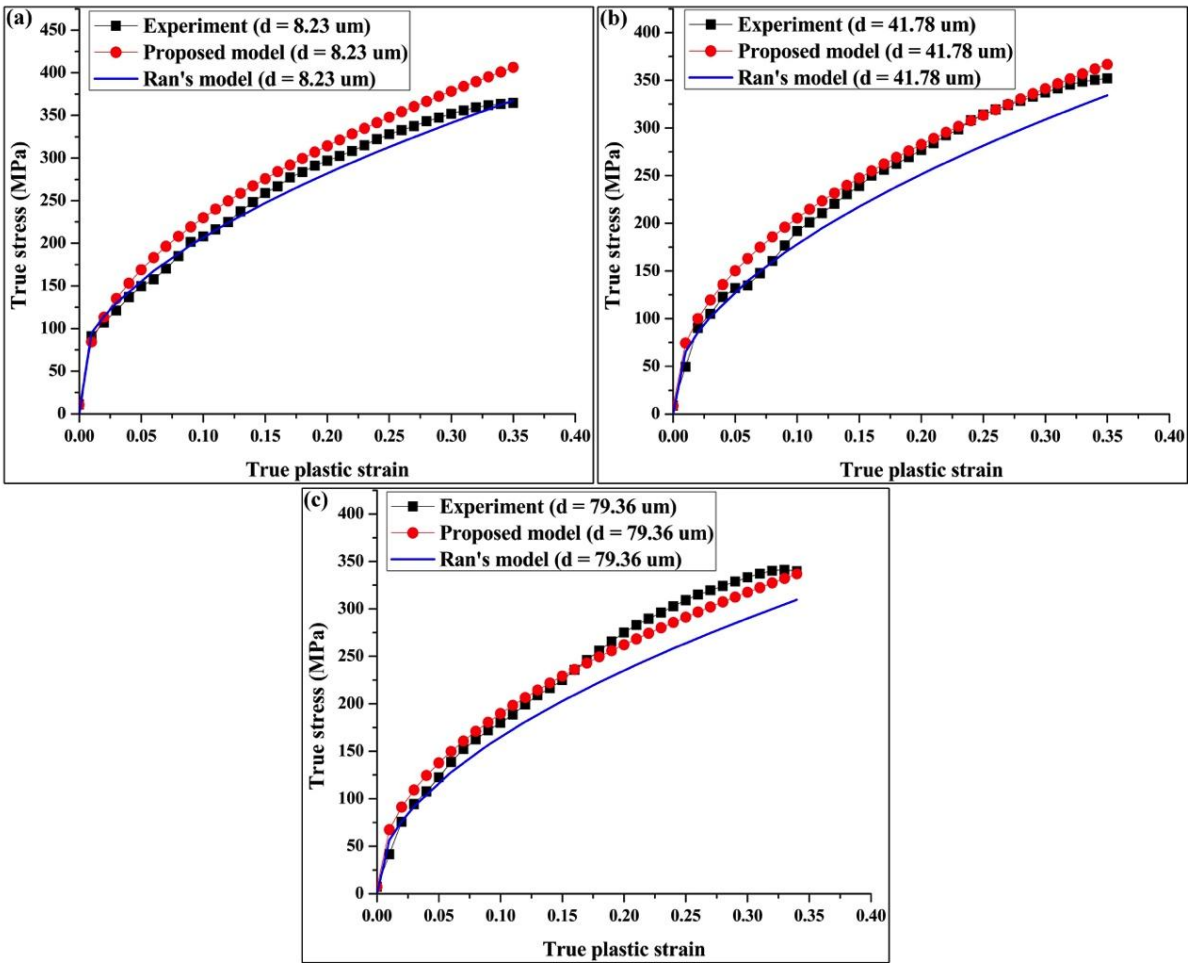

Fig. 11 Comparisons of experimental results and different constitutive models for the samples with different grain sizes. (a) d = 8.23 um; (b) d = 41.78 um and (c) d = 79.36 um.

4.2 Micro-tensile test

In order to validate the newly combined constitutive model, the micro-tensile specimens with different shapes designated as Type I, II and III made of the material with three grain sizes are employed, as shown in Fig. 12. The effective dimension at the sample center is 1 mm. The simulated results on the basis of the combined constitutive model are compared with the physical experiments of the micro-tensile tests using the prepared specimens. The FE simulations are conducted in ABAQUS with the powerful nonlinear analysis modules. The true stress and strain values of the deforming material are calculated based on the combined constitutive model, input and assigned to the three different geometrical shapes of specimens to facilitate the simulations. An axisymmetric model is built and the specimens of Types I, II and III are meshed with 9166, 10272 and 18939 elements of the 4-node bilinear element, CAX4R, and 9460, 10506 and 19199 nodes, respectively. Figs. 13, 14 and 15 compare the simulated load-displacement relationships with the physical experiments for the three different geometrical shapes of specimens with the grain sizes of 8.23, 41.78 and 79.36 um, respectively. It is apparent that the simulated load-displacement relationships match well with the experimental results of the specimens with the grain sizes of 41.78 and 79.36 um for all the three types. Although the trends of load-displacement curves predicted by simulations and the physical experiments of the specimens with the grain size of 8.23 um for all the three types are same, there is an obvious deviation for the central part of the curves. The main reason is that the fitting true stress-strain relationship based on the proposed constitutive model in Fig. 11(a) is larger than the experimental result. The larger fitting data result from the recalculation and adjustment of the newly combined constitutive model, which seek to reduce deviation from the physical experiments of all the specimens, also reported by Ran et al. [18]. Therefore, the comparisons of the simulated load-displacement relationships and the experimental results for the three different types of specimens with the grain sizes of 8.23,

41.78 and 79.36 um, respectively obviously indicate that the newly combined constitutive model considering the composition of grain interior, surface grain and grain boundary of materials is validated.

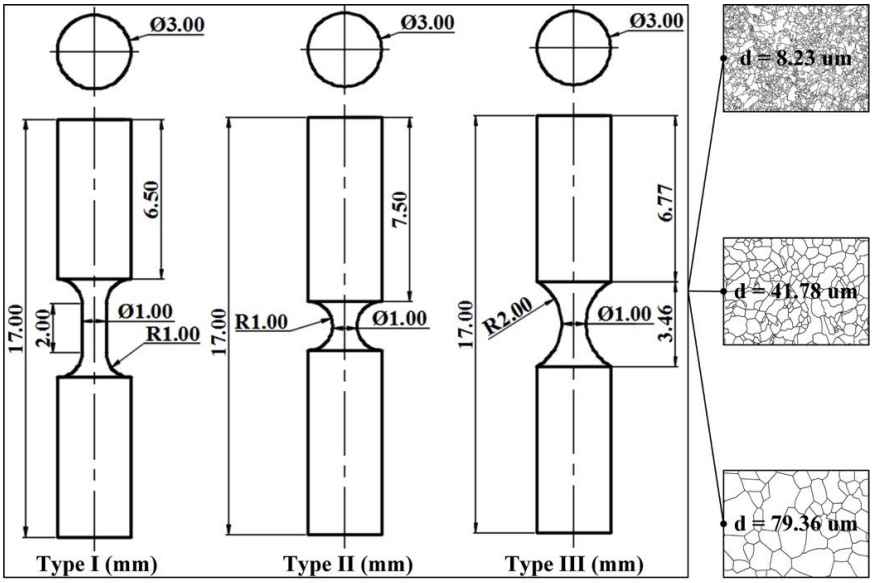

Fig. 12 Dimensions of the specimens with three different geometrical shapes and grain sizes.

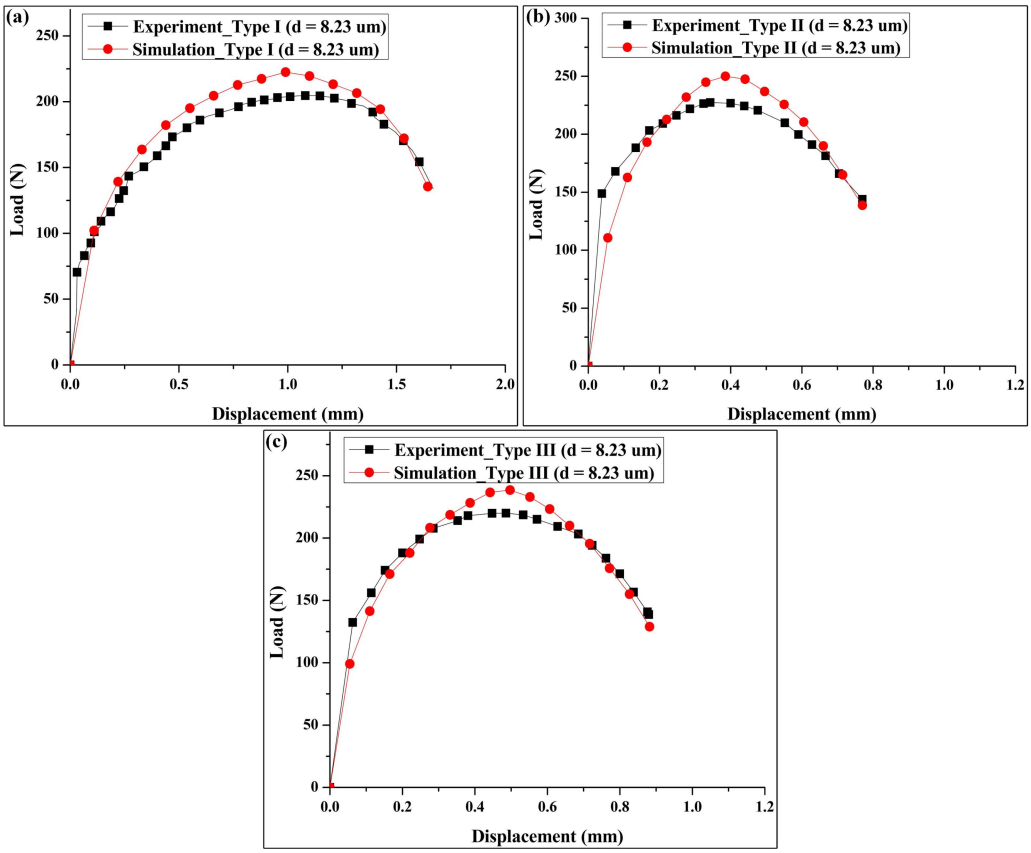

Fig. 13 Comparisons of experimental data and simulation of the specimen with the grain size of 8.23 um. (a) Type I; (b) Type II and (c) Type III.

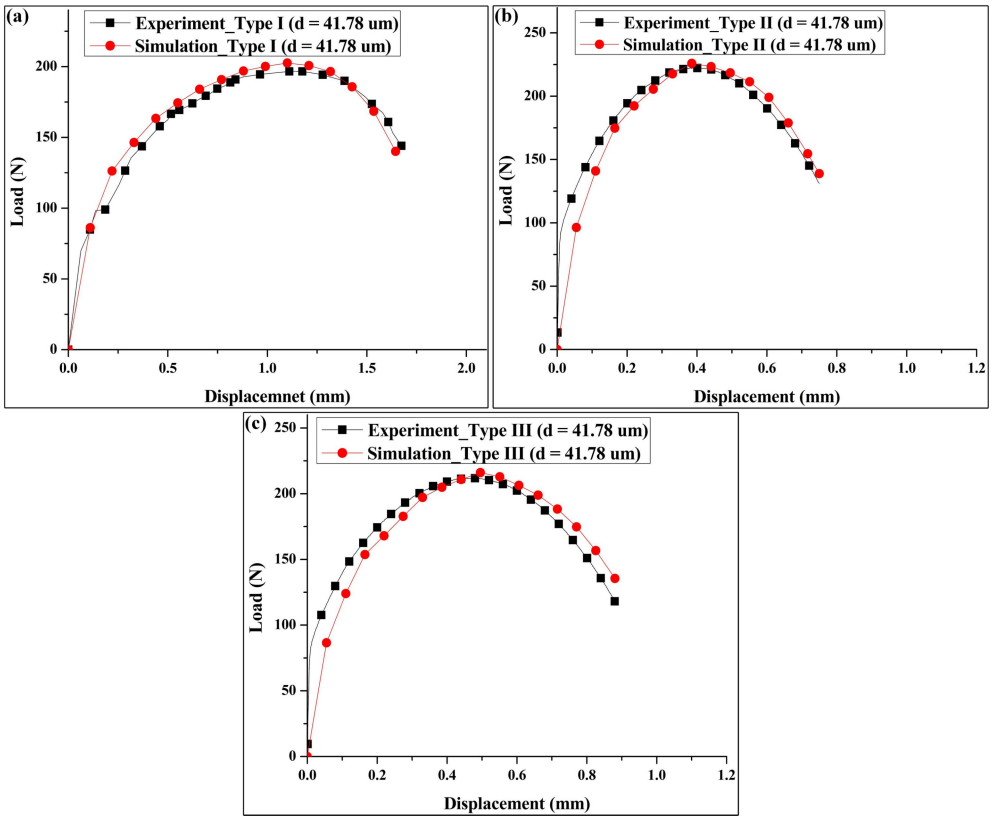

Fig. 14 Comparisons of experimental data and simulation of the specimen with the grain size of 41.78 um. (a) Type I; (b) Type II and (c) Type III.

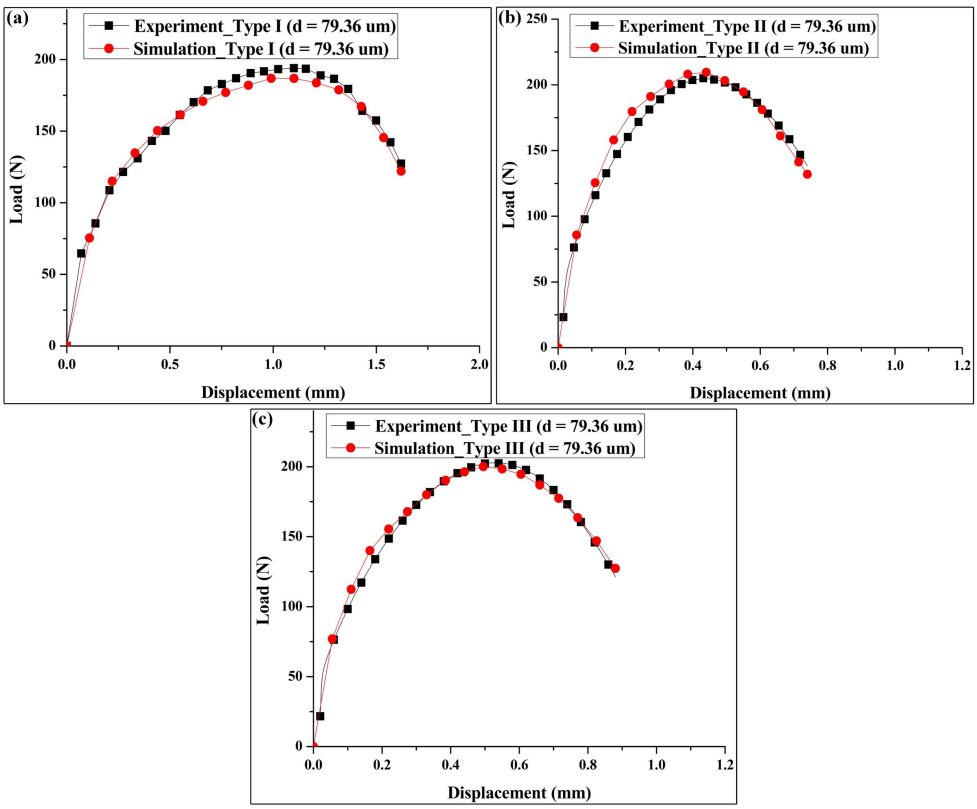

Fig. 15 Comparisons of experimental data and simulation of the specimen with the grain size of 79.36 um. (a) Type I; (b) Type II and (c) Type III.

5. Results and discussion

5.1 Stress triaxiality and fracture strain in micro-scale plastic deformation

The qualitative agreement of the experimental and simulated load-displacement relationships for the specimens with different geometrical shapes and microstructural grain sizes can facilitate the investigation on ductile fracture by using the newly combined constitutive model in micro-scale plastic deformation. The displacement at which the fracture happens is determined by the obvious drop of loading for all the cases in this research. The maximum equivalent plastic strain from simulation at fracture displacement is approximately regarded as fracture strain [33]. In addition, the stress triaxiality η is defined as follows:

$$\eta = \frac{\sigma_m}{\bar{\sigma}} \tag{15}$$

where $\sigma_m = \frac{1}{3}(\sigma_1 + \sigma_2 + \sigma_3)$ is the mean stress and $\bar{\sigma} = \sqrt{\frac{1}{2}[(\sigma_1-\sigma_2)^2+(\sigma_1-\sigma_3)^2+(\sigma_2-\sigma_3)^2]}$ is the equivalent von Mises stress.

According to the simulated results by employing the newly combined constitutive model, the curves of equivalent plastic strain and stress triaxiality at the central point of Type II specimens with different grain sizes which receives the maximum equivalent plastic strain are denoted by Fig. 16. It displays that the maximum equivalent plastic strain decreases with the increased grain size, while the stress triaxiality fluctuates against each other, particularly during the necking deformation stage. In addition, the shape of the deformed specimen determined by simulation agrees with that of the physical experiment for points A and B. It also suggests that the developed constitutive model can simulate the deformation process of micro-tensile test with sufficient accuracy. Fig. 17 reveals the change of stress triaxiality and fracture strain for the specimens with different geometrical shapes and grain sizes. For the specimens with a specified shape, both of fracture strain and stress triaxiality decrease with

the increased grain size, and the extent of the decreased stress triaxiality is obviously less than that of the decreased fracture strain. For the specimens with a specified grain size, fracture strain decreases with the increase of stress triaxiality, and the extent of the decreased fracture strain becomes gradually insignificant for the larger grain size. In addition, Type I specimen with the grain size of 8.23 um has the largest fracture strain and lower stress triaxiality. Type II specimen with the grain size of 79.36 um however has the smallest fracture strain and higher stress triaxiality. From the interaction among fracture strain, grain size and stress triaxiality in micro-scale deformation, it can be found that grain size has an influence on both stress triaxiality and fracture strain, and more significant on fracture strain. Moreover, high stress triaxiality causes the decreased fracture strain, and the extent of decreased fracture strain becomes subtler with the increased grain size. The increased stress triaxiality accelerates the growth and coalescence of microvoids. The specimen with high stress triaxiality is thus easier to fracture during plastic deformation. The finding that the extent of decreased fracture strain becomes subtler with the increased grain size could be attributed to the nonuniform distribution of grains and the inhomogeneous deformation. Chan and Fu [34] simulated that a large fraction of soft grains which deform along the loading direction in priority occur when the grain size increases and the number of grains decreases in the section of the specimen. A significantly localized deformation can be concentrated at the soft grains, which causes easier fracture during the plastic deformation. It further leads to the phenomenon that the extent of decreased fracture strain becomes subtler with the increased grain size. It facilitates to advance the knowledge of grain size effect and the impact of stress triaxiality on ductile fracture in micro-scale plastic deformation process.

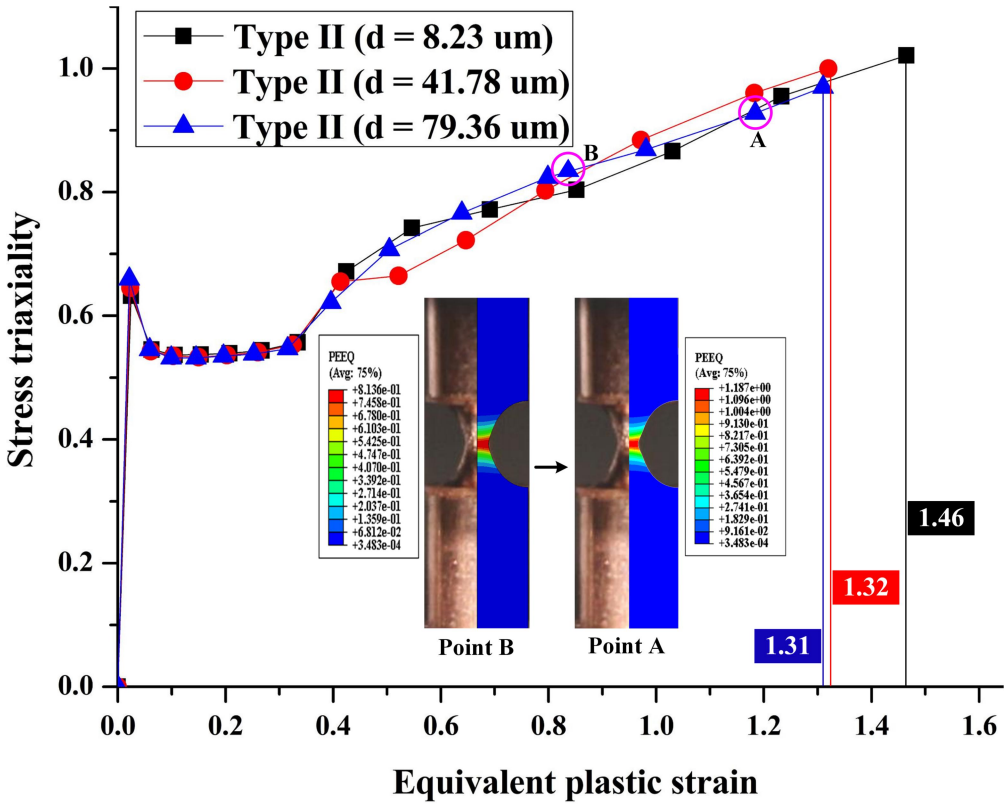

Fig. 16 Simulated stress triaxiality and equivalent plastic strain relationship.

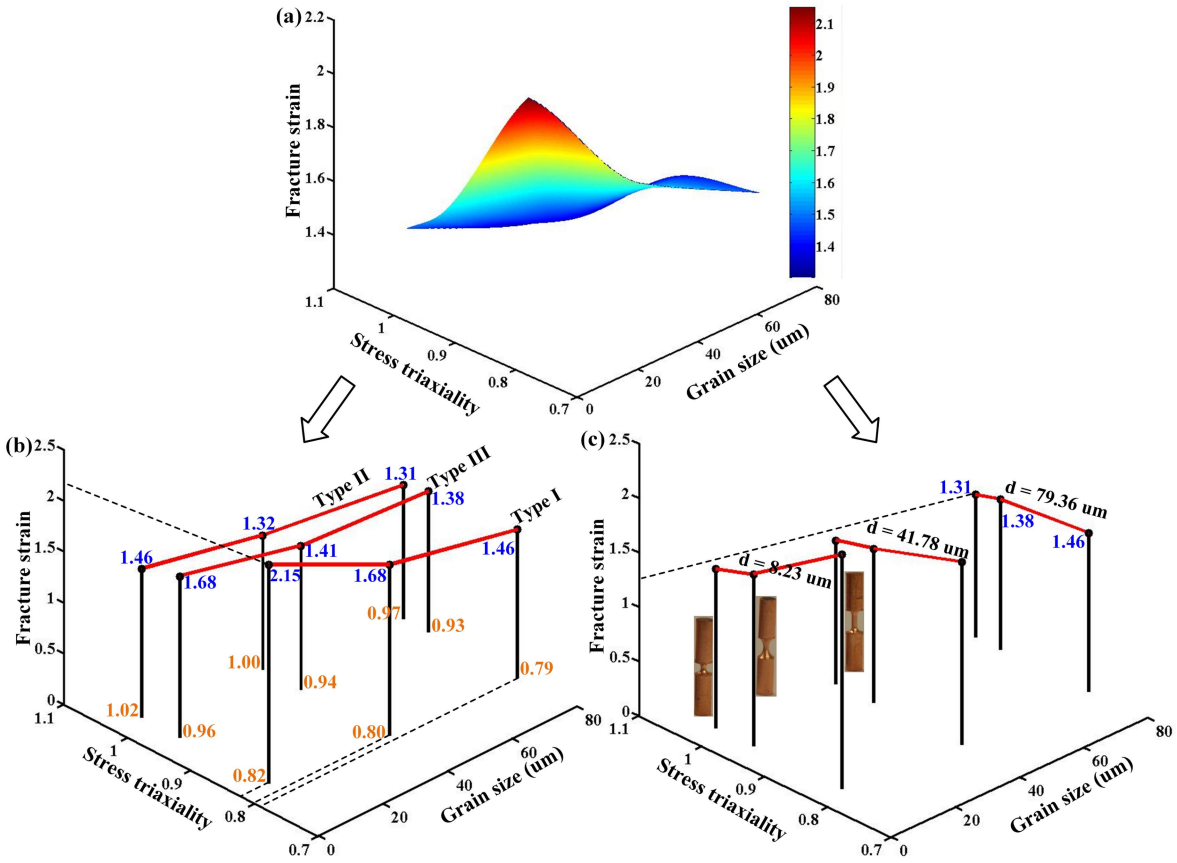

Fig. 17 The interaction among fracture strain, stress triaxiality and grain size. (a) 3D surface plot; (b) Specified shape and (c) Specified grain size.

5.2 Fractographs of the specimens with different geometrical shapes and grain sizes

The fracture surfaces of the specimens with different geometrical shapes and grain sizes are observed to study the fracture mode and mechanism in micro-scale plastic deformation. Figs. 18 and 19 present the scanning electron microscope (SEM) fractographs of the specimens with different grain sizes for a specified shape and with different geometrical shapes for a specified grain size, respectively. The 'cup and cone' fracture in which the 'cup' with the flat surface is dominated by the dimple fracture, and the 'cone' with shear lip is dominated by the shear fracture occurs in all the specimens. For the Type II specimens, the equiaxed dimples are fewer in number, more uneven in distribution, larger difference in size and deeper in depth for large dimple with the increased grain size. The shear fracture increasingly dominates as well. According to the ductile fracture mechanisms with different stress triaxiality levels experimentally studied by Barsoum and Faleskog [35], the intervoid shearing mechanism occurs at low stress triaxiality, while the necking of intervoid ligament appears at high stress triaxiality. The change of ductile fracture mode from dimple-dominant fracture to shear-dominant fracture in the 'cup-cone' fracture thus reflects the finding that the stress triaxiality decreases with the increased grain size for the specimens with a specified shape. Furthermore, Fig. 19 shows that Type I specimen exhibits the finest dimples compared to Type II specimen, which reveals the largest dimples when the grain size keeps constant. The larger dimples of Type II specimen are mainly caused by the fact that the increased stress triaxiality accelerates the growth and coalescence of microvoids. The specimen with high stress triaxiality is thus easier to fracture during plastic deformation. It can also be employed to explain that the fracture strain decreases with the increased stress triaxiality for the specimens with a specified grain size.

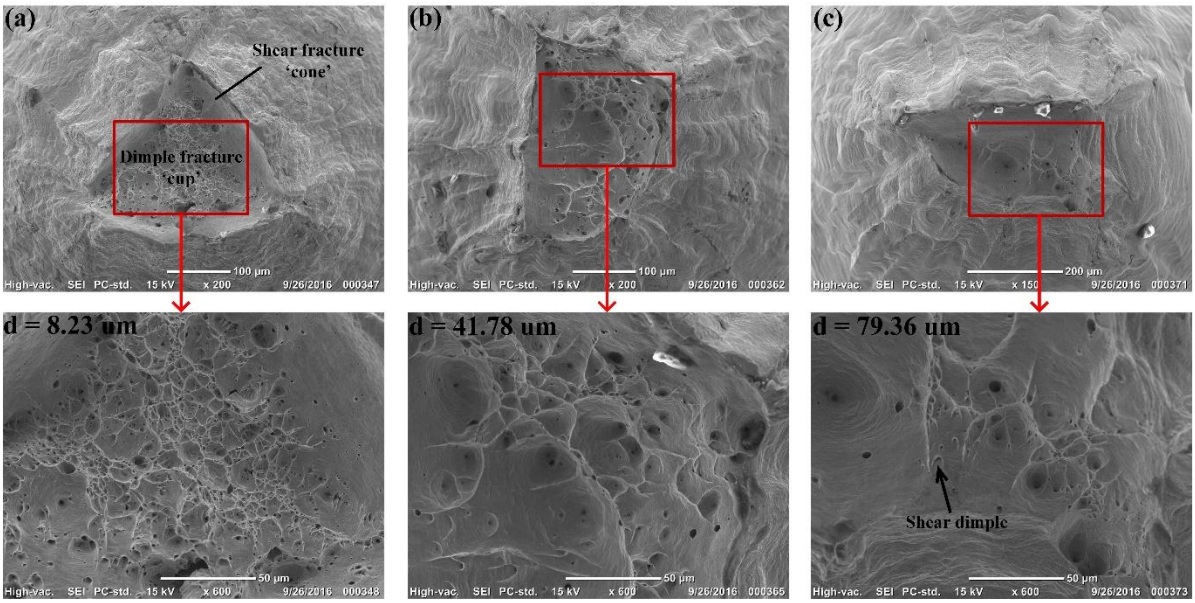

Fig. 18 Scanning electron microscope (SEM) fractographs of the specimens of Type II with different grain sizes. (a) d = 8.23 um; (b) d = 41.78 um and (c) d = 79.36 um.

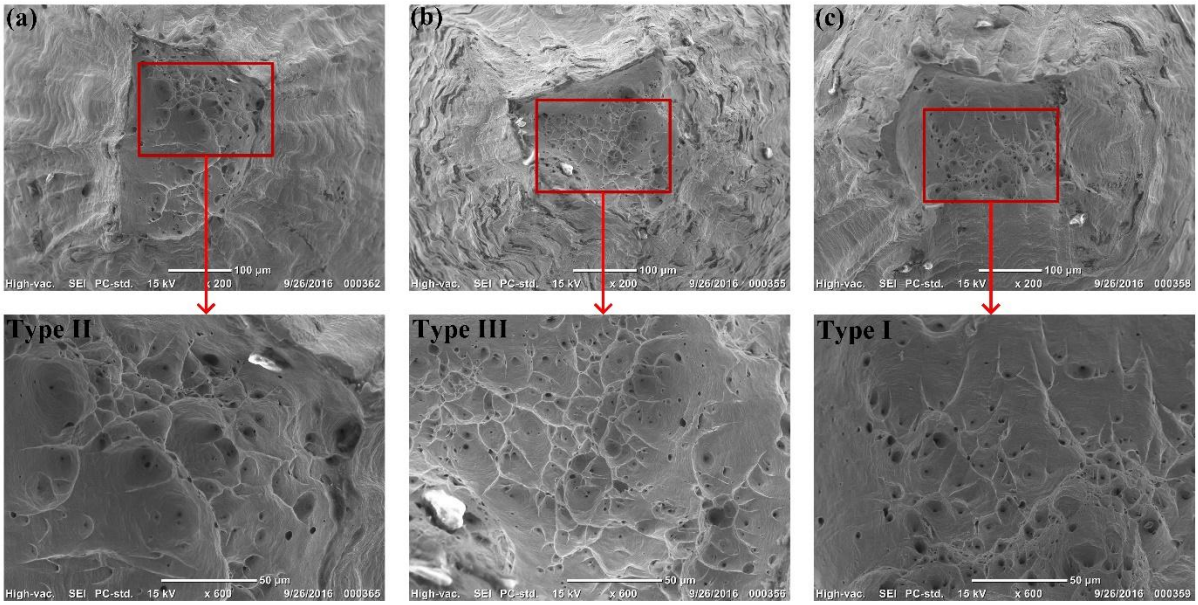

Fig. 19 SEM fractographs of the specimens of the grain size of 41.78 um with different shapes. (a) Type II; (b) Type III and (c) Type I.

6. Conclusions

In this research, a new constitutive model combining the surface layer and grain boundary strengthening models is built by taking into account of the contributions from grain interior,

surface grain and grain boundary to the deformation and ductile fracture in micro-scale plastic deformation. Its efficiency is thus validated via the experimental results and FE simulations of the micro-tensile specimens with three different geometrical shapes and grain sizes. The conclusions are drawn as follows:

(1) The newly combined surface layer and grain boundary strengthening model is validated by the good agreement between physical experiments and simulations. The proposed constitutive model can thus be used to analyze the deformation and ductile fracture more accurately in micro-scale deformation.

(2) The relationship of stress triaxiality, fracture strain and grain size is constructed based on the FE simulation by employing the newly combined constitutive model and physical experiment. It is found that both of stress triaxiality and fracture strain decrease with the increased grain size for the specimens with a specified shape. The fracture strain decreases with the increase of stress triaxiality for the specimens with a specified grain size.

(3) Grain size has an influence on both stress triaxiality and fracture strain, and more significantly on fracture strain. Moreover, high stress triaxiality causes the decrease of fracture strain, and the extent of decreased fracture strain becomes subtler with the increased grain size. In addition, fracture strain is larger when grain size is smaller and stress triaxiality is lower.

(4) The ‘cup-cone’ fracture exists in all the micro-tensile specimens. For the specimens with a specified shape, dimple-dominant fracture occurs at high stress triaxiality when the grain size is small, whereas shear-dominant fracture exists at low stress triaxiality when the grain size is large. For the specimens with a specified grain size, increased stress triaxiality accelerates the growth and coalescence of microvoids to make the larger dimples to fracture easily.

Acknowledgements

The authors gratefully acknowledge the funding support from the National Natural Science Foundation of China with the project of 51575465 and the project of B-Q55M (152792/16E) from the RGC of Hong Kong Government.

References

[1] Geiger M, Kleiner M, Eckstein R, Tiesler N and Engel U. Microforming. CIRP Ann Manuf Tech 2001;50(2):445-462.
[2] Fu MW and Chan WL. A review on the state-of-the-art microforming technologies. Int J Adv Manuf Tech 2013;67(9):2411-2437.
[3] Lassance D, Farègue D, Delannay F and Pardoen T. Micromechanics of room and high temperature fracture in 6xxx Al alloys. Prog Meter Sci 2007;52:62-129.
[4] Li H, Fu MW, Lu J, and Yang H, Ductile fracture: experiments and computations. Int J Plast 2011;27:147-180.
[5] Pineau A, Benzerga AA and Pardoen T. Failure of metals I: brittle and ductile fracture. Acta Mater 2016;107:424-483.
[6] Wen J, Huang Y, Hwang KC, Liu C and Li M. The modified Gurson model accounting for the void size effect. Int J Plast 2005;21:381-395.
[7] Vollertsen F, Biermann D, Hansen HN, Jawahir IS and Kuzman K. Size effects in manufacturing of metallic components. CIRP Ann Manuf Tech 2009;58(2):566-587.
[8] Lai XM, Peng LF, Hu P, Lan SH and Ni J. Material behavior modelling in micro/meso-scale forming process with considering size/scale effects. Comput Mater Sci 2008;43(4):1003-1009.
[9] Shen Y and Yu HP. Construction of a composite model of decreasing flow stress scale effect. J Mater Process Tech 2009;209(17):5845-5850.
[10] Liu JG, Fu MW, and Chan WL. A constitutive model for modeling of the deformation behavior in microforming with a consideration of grain boundary strengthening. Comput Mater Sci 2012;55:85-94.
[11] Deng YJ, Peng LF, Lai XM, Fu MW and Lin ZQ. Constitutive modeling of size effect on deformation behaviors of amorphous polymers in micro-scaled deformation. Int J Plast 2017;89:197-222.
[12] Ran JQ, Fu MW, and Chan WL. The influence of size effect on the ductile fracture in micro-scaled plastic deformation. Int J Plast 2013;41:65-81.
[13] Gruben G, Hopperstad OS and Børvik T. Evaluation of uncoupled ductile fracture criteria for the dual-phase steel Docol 600DL. Int J Mech Sci 2012;62(1):133-146.
[14] Toulfatzis AI, Pantazopoulos GA, and Paipetis AS. Fracture behavior and characterization of Lead-free brass alloys for machining applications. J Mater Eng Perform 2014;23:3193-3206.
[15] Das A, Das SK, and Tarafder S. Correlation of fractographic features with mechanical properties in systematically varied microstructures of Cu-strengthened high-strength low-alloy steel. Metall Mater Trans A 2009;40(13):3138-3146.

[16] Kim GY, Ni J, and Koç M. Modeling of the size effects on the behavior of metals in microscale deformation processes. J Manuf Sci Eng 2006;129(3):470-476.
[17] Armstrong R, Codd I, Douthwaite RM, and Petch NJ. The plastic deformation of polycrystalline aggregates. Philos Mag 1962;7(73):45-58.
[18] Ran JQ and Fu MW. A hybrid model for analysis of ductile fracture in micro-scaled plastic deformation of multiphase alloys. Int J Plast 2014;61:1-16.
[19] Clausen B, Lorentzen T, and Leffers T. Self-consistent modelling of the plastic deformation of f.c.c. polycrystals and its implications for diffraction measurements of internal stresses. Acta Mater 1998;46(9):3087-3098.
[20] Meyersm MA and Ashworth E. A model for the effect of grain size on the yield stress of metals. Philos Mag A 1982;46(5):737-759.
[21] Hirth JP. The influence of grain boundaries on mechanical properties. Metall Trans 1972;3(12):3047-3067.
[22] Chan WL and Fu MW. Experimental studies and numerical modeling of the specimen and grain size effects on the flow stress of sheet metal in microforming. Mater Sci Eng: A 2011;528(25-26):7674-7683.
[23] Kocks UF. The relation between polycrystal deformation and single-crystal deformation. Metall Mater Trans 1970;1(5):1121-1143.
[24] Swygenhoven HV, Spaczer M, and Caro A. Microscopic description of plasticity in computer generated metallic nanophase samples: a comparison between Cu and Ni. Acta Mater 1999;47(10):3117-3126.
[25] Gleiter H. Nanostructured materials: basic concepts and microstructure. Acta Mater 2000;48(1):1-29.
[26] Donovan PE. A yield criterion for Pd40Ni40P20 metallic glass. Acta metall 1989;37(2):445-456.
[27] Drucker DC. Some implications of work hardeinging and ideal plasticity. Quart Appl Math 1950;7(4):411-418.
[28] Jiang B and Weng GJ. A generalized self-consistent polycrystal model for the yield strength of nanocrystalline materials. J Mech Phys Solids 2004;52(5):1125-1149.
[29] Jiang B. A theory of compressive yield strength of nano-grained ceramics. Int J Plast 2004;20(11):2007-2026.
[30] Zhou J, Li Z, Zhu R, Li Y and Zhang Z. A mixtures-based model for the grain size dependent mechanical behavior of nanocrystalline materials. J Mater Process Tech 2008;197(1-3):325-336.
[31] Weng GJ. A micromechanical theory of grain-size dependence in metal plasticity. J Mech Phys Solids 1983;31(3):193-203.
[32] Chan WL, Fu MW and Yang B. Experimental studies of the size effect affected microscale plastic deformation in micro upsetting process. Mater Sci Eng: A 2012;534:374-383.
[33] Lou Y and Huh H. Prediction of ductile fracture for advanced high strength steel with a new criterion: experiments and simulation. J Mater Process Tech 2013;213(8):1284-1302.
[34] Chan WL and Fu MW. Experimental and simulation based study on micro-scaled sheet metal deformation behavior in microembossing process. Mater Sci Eng: A 2012;556:60-67.
[35] Barsoum I and Faleskog J. Rupture mechanisms in combined tension and shear—experiments. Int J Solids Struct 2007;44(6):1768-1786.